CONTINUATION ALONG BIFURCATION BRANCHES FOR A TUMOR MODEL WITH A NECROTIC CORE

WENRUI HAO*, JONATHAN D. HAUENSTEIN†, BEI HU‡, YUAN LIU§, ANDREW J. SOMMESE¶, AND YONG-TAO ZHANG‖

Abstract. We consider a free boundary problem for a system of partial differential equations, which arises in a model of tumor growth with a necrotic core. For any positive number R and $0 < \rho < R$, there exists a radially symmetric stationary solution with tumor free boundary $r = R$ and necrotic free boundary $r = \rho$. The system depends on a positive parameter μ, which describes tumor aggressiveness, and for a sequence of values $\mu_2 < \mu_3 < \cdots$, there exist branches of symmetry-breaking stationary solutions, which bifurcate from these values. Upon discretizing this model, we obtain a family of polynomial systems parameterized by μ. By continuously changing μ using a homotopy, we are able to compute nonradial symmetric solutions. We additionally discuss linear stability of such solutions.

Key words. Bifurcation, free boundary problem, polynomial systems, homotopy continuation, tumor model, necrotic core

Introduction. Tumor growth models are challenging both from a theoretic and numerical standpoint. These models determine free boundary problems where the changing shape of the tumor is of prime importance. Spherical solutions are given explicitly by analytical formulas in [21]. Analytically finding nonspherical solutions on a branch far from a spherical solution is intractable. Another difficult question is to determine the stability of each solution, which will tell us whether the tumor is likely to spread. It is established in [21] that for a sequence of values $\mu_2 < \mu_3 < \cdots$, the radially symmetric solutions bifurcate into nonradially symmetric ones. The nonradial solutions near the bifurcation point are known up to the first order.

Even though this article studies a tumor growth model with a necrotic core, we propose a general numerical algorithmic approach to answer the following: numerically compute values of the parameter where bifurcation occurs; numerically compute nonspherical solutions on a branch far from a spherical solution; and determine stability of these solutions. The theoretical analysis of the bifurcation values $\mu = \mu_l$ provided in [21] allows us to check our numerical approach in this situation.

The numerical algorithm we propose is based on recent developments in numerical algebraic geometry [4, 5, 24] and uses Bertini [3], a software package that implements numerical algebraic geometric algorithms. Roughly speaking, tumor models lead to systems of partial differential equations. We discretize these differential equations by

*Department of Applied and Computational Mathematics and Statistics, University of Notre Dame, Notre Dame, IN 46556 (whao@nd.edu). This author was supported by the Duncan Chair of the University of Notre Dame and NSF grant DMS-0712910.

†Department of Mathematics, Mailstop 3368, Texas A&M University, College Station, TX 77843 (jhauenst@math.tamu.edu, www.math.tamu.edu/∼jhauenst). This author was supported by Texas A&M University and NSF grant DMS-0915211.

‡Department of Applied and Computational Mathematics and Statistics, University of Notre Dame, Notre Dame, IN 46556 (b1hu@nd.edu, www.nd.edu/∼b1hu).

§Department of Applied and Computational Mathematics and Statistics, University of Notre Dame, Notre Dame, IN 46556 (yliu7@nd.edu).

¶Department of Applied and Computational Mathematics and Statistics, University of Notre Dame, Notre Dame, IN 46556 (sommese@nd.edu, www.nd.edu/∼sommese). This author was supported by the Duncan Chair of the University of Notre Dame and NSF grant DMS-0712910.

‖Department of Applied and Computational Mathematics and Statistics, University of Notre Dame, Notre Dame, IN 46556 (yzhang10@nd.edu). This author was partially supported by NSF grant DMS-0810413

incorporating the shape of the tumor utilizing a floating mesh with grid points on the moving boundary of the tumor. This leads to a system consisting of thousands of multivariate polynomials. To find bifurcation points of the spherical solutions as the tumor-aggressiveness factor μ changes, we track the spherical solution using μ as a continuation parameter monitoring the condition number of the Jacobian of the general system for not-necessarily-spherical solutions. Since the system must be degenerate, the condition number must be infinite at the bifurcation points. Due to this rank deficiency, the computation requires using adaptive multiprecision pathtracking [4, 5], a feature currently only available with Bertini, to perform computations in small neighborhoods of the bifurcation. Using a numerical approximation of the bifurcation point, we approximate the tangent cone to the family of solutions at the bifurcation point. Upon computing the tangent directions of the nonspherical branch, we can use continuation to numerically track along the branch and compute the nonradially symmetric solutions far along the branch. We also determine the linear stability of these solutions.

1. The model. Mathematical models of solid tumor growth, which consider the tumor tissue as a density of proliferating cells, have been developed and studied in many papers; see [1, 2, 6, 7, 8, 10, 12, 13, 14, 16, 17, 19, 20, 22, 23] and the references provided in them. Radially symmetric solutions have been extensively discussed . A spherical shape models the tumors grown in vitro, but tumors in vivo may develop protrusions. It is therefore interesting to explore the existence of nonspherical solutions of tumor models.

If dead cells are not removed in an efficient manner from the tumor, they accumulate inside to form a necrotic core [10, 12]. A necrotic tumor growth model consists of a core of necrotic cells and a shell adjacent to this necrotic core of proliferating cells. In particular, let $\Omega(t)$ denote the tumor domain at time t, and $D(t) \subset \Omega(t)$ be the necrotic core within the tumor domain.

Let p denote the pressure within the tumor resulting from the proliferation of the tumor cells, σ denote the concentration of nutrients. Then a model with necrotic core is derived in [10, 12], see also [21]. The steady-state system of the tumor model with a necrotic core is given as follows(see [21])

$$\Delta\sigma = \sigma\chi(x) \qquad \text{in } \Omega, \tag{1.1}$$

$$-\Delta p = \mu(\sigma - \widetilde{\sigma})\chi(x) \quad \text{in } \Omega, \tag{1.2}$$

$$\sigma = \underline{\sigma} \qquad \text{in } \partial D, \tag{1.3}$$

$$\sigma = 1 \qquad \text{on } \partial\Omega, \tag{1.4}$$

$$p = \kappa \qquad \text{on } \partial\Omega, \tag{1.5}$$

$$\frac{\partial p}{\partial n} = 0 \qquad \text{on } \partial\Omega, \tag{1.6}$$

where $\underline{\sigma}$ is a constant density of cells in the necrotic core, $\widetilde{\sigma} > 0$ is a threshold concentration, $\underline{\sigma} < \widetilde{\sigma} < 1$ and μ is a positive parameter measuring the aggressiveness of the tumor.

2. Discretization. To demonstrate the applicability of numerical algebraic geometric methods to study free boundary problems, we will first describe how we generated a polynomial system by discretizing a 2-dimensional steady-state necrotic tumor model. Since this model has two free boundaries, we developed a novel approach to allow the grid to change in coordination with the two boundaries.

Let N_θ denote the number of fixed directions and $\theta_i = i \cdot \frac{2\pi}{N_\theta}$ for $i = 0, \ldots, N_\theta - 1$. Let r_i and ρ_i be the distance from the origin to the boundary of the tumor and the boundary of the necrotic core, respectively, in the θ_i direction. That is, r_i and ρ_i model the two free boundaries in the θ_i direction and can change independently.

We then discretize in each of these fixed directions both the necrotic region and the tumor region. Let N_ρ be the number of equally spaced grid points between the origin and each ρ_i and N_r be the number of equally spaced grid points between each ρ_i and r_i. Near the boundary of the tumor, we added two additional grid points that improve the accuracy of the discretization.

The location of all of the grid points change in accordance with the changing boundaries. For example, Figure 2.1 presents the grid for a radial solution using $N_\theta = 40$, $N_\rho = 5$, and $N_r = 12$. Using the same setup, Figure 2.2 presents a grid for a nonradial solution. The red curve inside the region is the location of the necrotic core boundary.

FIG. 2.1. *Plot of a radially symmetric grid with* $N_\theta = 40$, $N_\rho = 5$, *and* $N_r = 12$

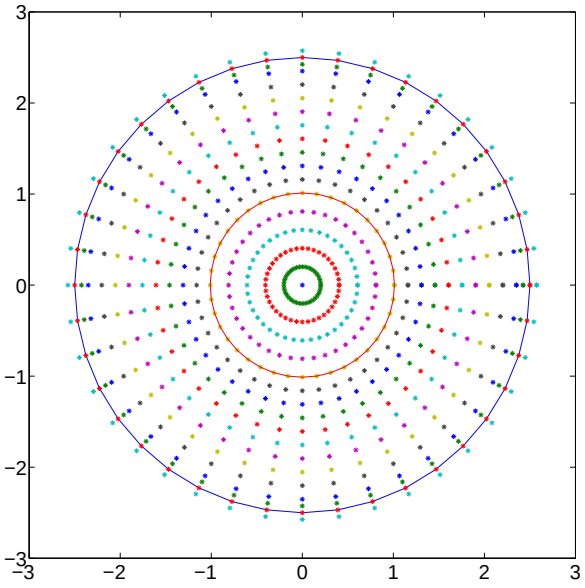

We discretized the model described by (1.1–1.6) based on this moving grid using a third order finite difference scheme. The stencil of grid points consisted of the center point together with 14 surrounding points, which is presented in Figure 2.3.

Using this stencil, we will now explicitly describe the discretization of σ with the discretization for p following similarly. To simplify, we will denote the location center grid point of the stencil as the origin. Let $d_{i,j}$ denote the distance from the j^{th} grid point along the i^{th} angular direction to the origin. The Taylor series expansion using

FIG. 2.2. *Plot of a nonradially symmetric grid with* $N_\theta = 40$, $N_\rho = 5$, *and* $N_r = 12$

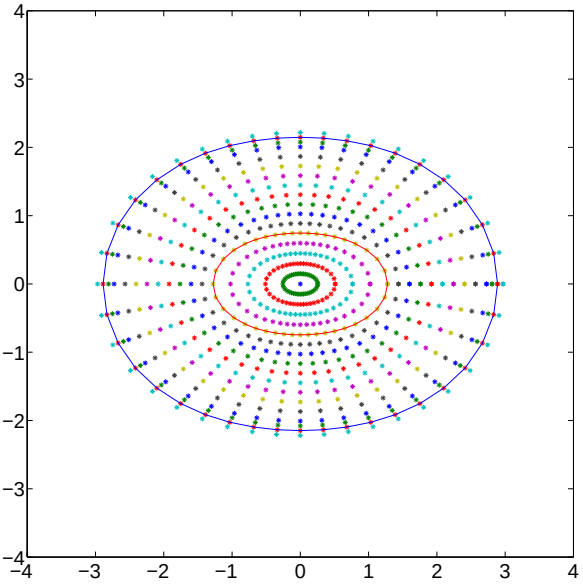

the surrounding grid points and values of σ yield a linear system

$$\begin{bmatrix} d_r(0,-2) & 0 \\ d_r(0,-1) & 0 \\ d_r(0,1) & 0 \\ d_r(0,2) & 0 \\ d_r(-2,0) & d_\theta(-2,0) \\ d_r(-1,0) & d_\theta(-1,0) \\ d_r(1,0) & d_\theta(1,0) \\ d_r(2,0) & d_\theta(2,0) \\ d_r(-2,-1) & d_\theta(-2,-1) \\ d_r(-1,-1) & d_\theta(-1,-1) \\ d_r(1,-1) & d_\theta(1,-1) \\ d_r(2,-1) & d_\theta(2,-1) \\ d_r(-1,-2) & d_\theta(-1,-2) \\ d_r(1,-2) & d_\theta(1,-2) \end{bmatrix} \begin{bmatrix} \partial_r^{i,j}\sigma \\ \partial_{rr}^{i,j}\sigma \\ \partial_{rrr}^{i,j}\sigma \\ \partial_{rrrr}^{i,j}\sigma \\ \partial_\theta^{i,j}\sigma \\ \partial_{\theta\theta}^{i,j}\sigma \\ \partial_{r\theta}^{i,j}\sigma \\ \partial_{rr\theta}^{i,j}\sigma \\ \partial_{r\theta\theta}^{i,j}\sigma \\ \partial_{\theta\theta\theta}^{i,j}\sigma \\ \partial_{r\theta\theta\theta}^{i,j}\sigma \\ \partial_{rr\theta\theta}^{i,j}\sigma \\ \partial_{rrr\theta}^{i,j}\sigma \\ \partial_{\theta\theta\theta\theta}^{i,j}\sigma \end{bmatrix} = \begin{bmatrix} \sigma_{0,-2} - \sigma_{0,0} \\ \sigma_{0,-1} - \sigma_{0,0} \\ \sigma_{0,1} - \sigma_{0,0} \\ \sigma_{0,2} - \sigma_{0,0} \\ \sigma_{-2,0} - \sigma_{0,0} \\ \sigma_{-1,0} - \sigma_{0,0} \\ \sigma_{1,0} - \sigma_{0,0} \\ \sigma_{2,0} - \sigma_{0,0} \\ \sigma_{-2,-1} - \sigma_{0,0} \\ \sigma_{-1,-1} - \sigma_{0,0} \\ \sigma_{1,-1} - \sigma_{0,0} \\ \sigma_{2,-1} - \sigma_{0,0} \\ \sigma_{1,-2} - \sigma_{0,0} \\ \sigma_{-1,-2} - \sigma_{0,0} \end{bmatrix},$$

where

$$d_r(i,j) = \left[d_{i,j}, \frac{d_{i,j}^2}{2}, \frac{d_{i,j}^3}{3!}, \frac{d_{i,j}^4}{4!} \right]$$

and

$$\begin{aligned} &d_\theta(i,j) \\ &= \left[i\Delta\theta, \tfrac{(i\Delta\theta)^2}{2}, i\Delta\theta d_{i,j}, \tfrac{d_{i,j}^2 i\Delta\theta}{2}, \tfrac{d_{i,j}(i\Delta\theta)^2}{2}, \tfrac{(i\Delta\theta)^3}{3!}, \tfrac{d_{i,j}(i\Delta\theta)^3}{3!}, \tfrac{d_{i,j}^2(i\Delta\theta)^2}{4}, \tfrac{d_{i,j}^3 i\Delta\theta}{3!}, \tfrac{(i\Delta\theta)^4}{4!} \right], \end{aligned}$$

We obtain derivatives by solving linear system. Higher derivatives are only part of computation and are not used in discretization. Here we list the first and second derivatives with respect to r. The derivatives with respect to θ are complicated and available on http://www.nd.edu/∼sommese/preprints/scheme.m.

$$\begin{aligned}
&\partial_r^{i,j}\sigma\\
&= \frac{d_{i,j+1}d_{i,j+2}d_{i,j-1}d_{i,j-2}}{(d_{i,j-1}-d_{i,j-2})}\sum_{k=1}^{2}(-1)^k\frac{\sigma_{0,-k}}{d_{i,j-k}^2(d_{i,j+1}-d_{i,j-k})(d_{i,j+2}-d_{i,j-k})}\\
&+\frac{d_{i,j-1}d_{i,j-2}d_{i,j+1}d_{i,j+2}}{(d_{i,j+1}-d_{i,j+2})}\sum_{k=1}^{2}(-1)^k\frac{\sigma_{0,k}}{d_{i,j+k}^2(d_{i,j+k}-d_{i,j-1})(d_{i,j+k}-d_{i,j-2})}\\
&-\Big(\frac{1}{d_{i,j+1}}+\frac{1}{d_{i,j+2}}+\frac{1}{d_{i,j-1}}-\frac{1}{d_{i,j-2}}\Big)\sigma_{0,0}
\end{aligned}$$

$$\begin{aligned}
&\partial_{rr}^{i,j}\sigma\\
&=2\Big(\frac{d_{i,j+2}+d_{i,j-2}}{d_{i,j+2}d_{i,j-1}^2+d_{i,j-1}^2d_{i,j-2}-d_{i,j-1}^3-d_{i,j-2}d_{i,j-1}d_{i,j+2}}\\
&+\frac{d_{i,j-1}d_{i,j+2}+d_{i,j-2}d_{i,j+2}+d_{i,j-1}d_{i,j-2}}{d_{i,j-1}(d_{i,j+1}-d_{i,j-1})(d_{i,j+2}-d_{i,j-1})(d_{i,j-1}-d_{i,j-2})}\Big)\sigma_{0,-1}\\
&-2\frac{d_{i,j+2}d_{i,j+1}+d_{i,j-1}d_{i,j+1}+d_{i,j+2}d_{i,j-1}}{d_{i,j-2}(d_{i,j+1}-d_{i,j-2})(d_{i,j+2}-d_{i,j-2})(d_{i,j-1}-d_{i,j-2})}\sigma_{0,-2}\\
&-2\frac{-d_{i,j+2}^3d_{i,j-1}^2+d_{i,j+2}^3d_{i,j-2}^2+d_{i,j+2}^2d_{i,j-1}^3-d_{i,j+2}^2d_{i,j-2}^3-d_{i,j-1}^3d_{i,j-2}^2+d_{i,j-2}^3d_{i,j-1}^2}{d_{i,j+1}(d_{i,j+1}-d_{i,j+2})(d_{i,j+1}-d_{i,j-1})(d_{i,j+1}-d_{i,j-2})(d_{i,j+2}-d_{i,j-1})}\\
&\cdot\frac{\sigma_{0,1}}{(d_{i,j+2}-d_{i,j-2})(d_{i,j-1}-d_{i,j-2})}\\
&-2\frac{d_{i,j+1}d_{i,j-1}+d_{i,j-2}d_{i,j+1}+d_{i,j-2}d_{i,j-1}}{d_{i,j+2}(d_{i,j+1}-d_{i,j+2})(d_{i,j+2}-d_{i,j-1})(d_{i,j+2}-d_{i,j-2})}\sigma_{0,2}\\
&2\Big(\frac{d_{i,j+1}+d_{i,j+2}+d_{i,j-1}}{d_{i,j+1}d_{i,j+2}d_{i,j-1}}+\frac{d_{i,j+1}d_{i,j+2}+d_{i,j+1}d_{i,j-1}+d_{i,j+2}d_{i,j-1}}{d_{i,j+1}d_{i,j+2}d_{i,j-1}d_{i,j-2}}\Big)\sigma_{0,0}
\end{aligned}$$

The first derivatives with respect to r is represented by ∂_r^j and similar for the others. The first and second derivatives in θ direction are represented by $\partial_\theta^{i,j}$ and $\partial_{\theta\theta}^{i,j}$ respectively. The mixed derivatives are $\partial_{r\theta}^{i,j}$. The surrounding 14 points are showed in left and right part of Figure 2.3 for interior points and boundary points respectively.

To avoid numerical difficulties with polar coordinates at the origin, we utilized Cartesian coordinates together with a central difference scheme. The variables of the resulting discretized system correspond to the location of the free boundaries in each direction along with the concentration of nutrients and pressure at each grid point. In particular, the number of variables of discretized system is $N_\theta(2(N_\rho+N_R)+1)+2$. To be more specific, define $\sigma_{i,j}=\sigma(\theta_i,r_j)$ and $p_{i,j}=p(\theta_i,r_j)$, for $i=0,1,2,\ldots,N_\theta$

and $j = 0, 1, 2, \ldots, N_\rho + N_R$. The discretized system is

$$F(\sigma_{i,j}, p_{i,j}, r_i, \mu) = \begin{cases} \partial_{rr}^{i,j}\sigma + \frac{1}{r_{i,j}}\partial_r^{i,j}\sigma + \frac{1}{r_{i,j}^2}\partial_{\theta\theta}^{i,j}\sigma &= \sigma_{i,j}\chi(j > N_\rho), \\ -\left(\partial_{rr}^{i,j}p + \frac{1}{r_{i,j}}\partial_r^{i,j}p + \frac{1}{r_{i,j}^2}\partial_{\theta\theta}^{i,j}p\right) &= \mu(\sigma_{i,j} - \widetilde{\sigma})\chi(j > N_\rho), \\ \sigma_{i,N_\rho} &= \underline{\sigma}, \\ \sigma_{i,N_R} &= 1, \\ p &= \kappa, \\ \partial_r^j p \partial_r^j \sigma + \partial_\theta^{i,j} p \partial_\theta^{i,j} \sigma \frac{1}{r_{i,j}^2} &= 0, \\ \partial_r^{i,N_\rho} p^+ &= \partial_r^{i,N_\rho} p^-, \end{cases} \tag{2.1}$$

where

$$\kappa|_{\partial\Omega} = \frac{R(\partial_r^{i,N_R}\sigma)^2(R\partial_r^{i,N_R}\sigma + \partial_{\theta\theta}^{i,N_R}\sigma) + (\partial_\theta^{i,N_R}\sigma)^2(R\partial_{rr}^{i,N_R}\sigma + 2\partial_r^{i,N_R}\sigma) - 2R\partial_r^{i,N_R}\sigma\partial_\theta^{i,N_R}\sigma\partial_{r\theta}^{i,N_R}\sigma}{\left(\sqrt{(R\ \partial_r^{i,N_R}\sigma)^2 + (\partial_\theta^{i,N_R}\sigma)^2}\right)^3}.$$

All the numerical derivatives are obtained by the third order finite difference scheme, and $\partial_r^{i,N_\rho}p^+$ and $\partial_r^{i,N_\rho}p^-$ are two sided derivatives. It should be emphasized that derivatives from each side of the dead-core boundary are computed using only grid points from one side and therefore the jump of second derivatives of σ and p doesn't impact this numerical computation. Since the derivatives involve r_j, these are described by rational functions. Clearing the denominators yields a polynomial system parameterized by μ.

FIG. 2.3. *Stencil for third order scheme*

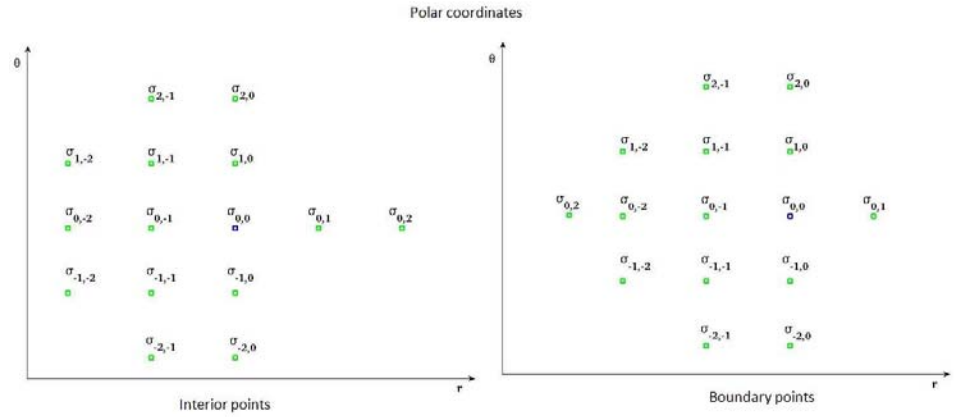

3. The bifurcation problem. Using the discretized problem described in Section 2, we want to numerically compute radially symmetric and nonradially symmetric solutions and, in particular, values of the parameter where bifurcations occur.

The first step is to compute radially symmetric solutions for some fixed radius R and given parameter $\underline{\sigma}$. In this case, each $r_i = R$ and $\rho_i = P$ for some radius $0 < P < R$. In the radially symmetric case, σ and p are independent of θ meaning

that the discretized polynomial system simplifies extensively. For a given value of μ, the resulting polynomial system can be solved using Bertini [3].

$$\left\{\begin{array}{rcl} \partial_{rr}^j\sigma + \frac{1}{r_j}\partial_r^j\sigma &=& \left\{\begin{array}{ll} \sigma_j, & j > N_\rho \\ 0, & j \le N_\rho \end{array}\right. \\ \partial_{rr}^j p + \frac{1}{r_j}\partial_r^j p &=& \left\{\begin{array}{ll} -\mu(\sigma_j - \widetilde{\sigma}), & j > N_\rho \\ 0, & j \le N_\rho \end{array}\right. \\ \sigma_{N_\rho} &=& \underline{\sigma}, \\ \sigma_{N_R} &=& 1, \\ p_{N_R} &=& \frac{1}{R}, \\ \partial_r^{N_R} p \ \partial_r^{N_R}\sigma &=& 0, \\ \partial_r^{N_\rho} p^+ &=& \partial_r^{N_\rho} p^-, \end{array}\right. \tag{3.1}$$

where

$$\partial_r^j\sigma = \left\{\begin{array}{ll} \dfrac{-\sigma_{0,2} + 8\sigma_{0,1} - 8\sigma_{0,-1} + \sigma_{0,-2}}{12\Delta R} & \text{interior points} \\ \dfrac{-\sigma_{0,2} + 20\sigma_{0,-1} + 16\sigma_{0,1} + 45\sigma_{0,0} - 80\sigma_{0,-2}}{30\Delta R} & \text{boundary point} \end{array}\right.$$

and

$$\partial_{rr}^j\sigma = \left\{\begin{array}{ll} \dfrac{-\sigma_{0,2} + 16\sigma_{0,1} + 16\sigma_{0,-1} - \sigma_{0,-2} - 30\sigma_{0,0}}{12\Delta R^2} & \text{interior points} \\ \dfrac{-\sigma_{0,2} + 10\sigma_{0,-1} + 56\sigma_{0,1} - 105\sigma_{0,0} + 40\sigma_{0,-2}}{15\Delta R^2} & \text{boundary point} \end{array}\right. .$$

It is similar for the derivatives of function p. Upon computing the radially symmetric solution for a given value of μ, the second step is to utilize the parameterization by μ of the polynomial system to determine the values where bifurcations occur. These values are located where the Jacobian of the discretized polynomial system is rank deficient. We utilized parameter continuation implemented in Bertini to look for such values by monitoring the condition number as μ varied. Figure 3.1 displays a graph of the condition number with respect to μ for $3 \le \mu \le 9$ where $R = 2.5$ and $\underline{\sigma} = 0.5$. In particular, we observe that the condition number spikes near $\mu = 7.98$ indicating the existence of a nearby singular radially symmetric solution. Since higher precision arithmetic is often needed near a singularity to maintain the integrity of the floating point computations, we used the adaptive precision path tracking algorithms of [4, 5] implemented in Bertini to control the precision utilized for this computation. All the computations discussed here were run on a 2.33 GHz Intel Xeon 5410 processor running 64-bit Linux. Table 3.1 gives the numerical error for computing μ_2 and time consumed. To determine the error in our numerical approximation, we compared the radially symmetric solution for $\mu = 8$ with the theoretical solution described in [21]. Table 3.2 displays the error for three different grids.

Given a numerical approximation of μ where the Jacobian is numerically rank deficient, the third step is to approximate the local tangent cone. This describes the tangent directions of the solution branches at the bifurcation. Due to the rank deficiency, this computation utilized multiprecision arithmetic. To simplify the notation, rewrite (2.1) as $F(x, \mu)$, where $x = (\sigma_{i,j}, p_{i,j}, r_i)$ for $i = 1, 2, \ldots, N_\theta$ and $j = 0, 1, \ldots, N_R + N_\rho$ are variables and μ is a parameter.

TABLE 3.1
Comparing (discretized) bifurcation value of μ_2 on a sequence of grids

Theoretical μ_2	N_θ	N_R	N_ρ	Numerical μ_2	Abs. error	Computing time
7.9772	40	10	5	7.9746	3e-3	30m29s
	48	12	6	7.9764	8e-4	41m54s
	64	16	8	7.9770	2e-4	70m23s

TABLE 3.2
Numerical error of radial symmetrical solution for $\mu = 8$ on a sequence of grids

N_θ	N_R	N_ρ	Numerical error
40	10	5	3.9876e-6
64	16	8	9.7339e-7
80	20	10	4.9838e-7

Given a polynomial system

$$f = \begin{bmatrix} f_1 \\ \vdots \\ f_m \end{bmatrix}$$

in $M+1$ variables and a solution x^*, the tangent cone is the set of common zeroes of the lowest order terms of the Taylor expansions at x^* of the elements of the ideal generated by the polynomials $f_1, \ldots, f_m$. This is at first sight a difficult computation. In the special case when the Jacobian J_f of f evaluated at x^* has rank $M-1$, then we know that the tangent cone lies in the two-dimensional linear space

$$\mathcal{V} := \left\{ v \in \mathbb{C}^{M+1} \mid J_f \cdot v = 0 \right\}.$$

If $\lambda \in \mathbb{C}^M$ is a nonzero row vector such that $\lambda \cdot J_f = 0$, it follows that all first order derivatives of $\lambda \cdot f$ vanish at x^*. We can compute the second order terms $\mathcal{Q}(x)$ of $\lambda \cdot f$ using the Hessian of $\lambda \cdot f$ at x^*. The tangent cone in question belongs to the solution set of $\mathcal{Q}$ on $\mathcal{V}$, and if this solution set is one-dimensional, it consists of either one or two lines. From this we conclude the tangent cone consists of at most two lines. In our case, using [21], we compute two lines, one in the direction of the radially symmetric branch and the other in the direction of the nonradially symmetric branch. We can use this direction with continuation to move onto the bifurcation branch.

The following algorithm computes these two tangent directions by reducing down to a polynomial in two variables utilizing an intrinsic parameterization of $\mathcal{V}$. The tangent directions then correspond to the two solutions of a polynomial system consisting of a homogeneous quadratic and a linear polynomial in two variables.

Procedure $(\Delta x_1, \Delta x_2) = \textbf{TangentCone}(F, \mu_0, x_0, \Delta_\mu)$
Input A parameterized polynomial system $F(x, \mu)$, a parameter value μ_0, a point x_0 that is a singular solution of $F(x, \mu_0)$, and expected variation Δ_μ.
Ouput Two tangent directions Δx_1 and Δx_2.
Begin

1. Compute the Jacobian matrix J_x with respect to the variables x and the derivative J_μ with respect to the parameter μ for F at (x_0, μ_0). Set $A := [J_x \ J_\mu]$.

FIG. 3.1. *Condition number with respect to μ for $R = 2.5$ and $\underline{\sigma} = 0.5$*

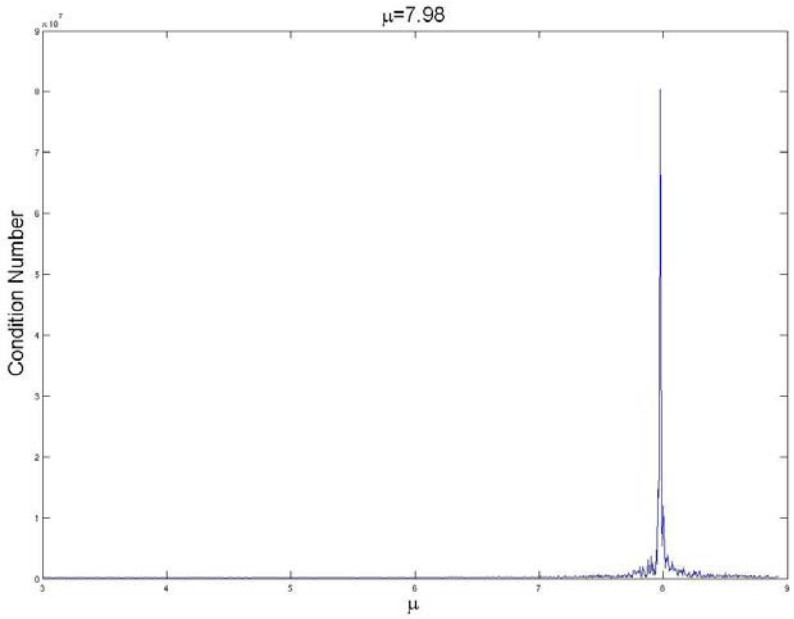

2. Compute a basis $\begin{bmatrix} q_1 & q_2 \\ u_1 & u_2 \end{bmatrix}$ for the two-dimensional null space of A and a nonzero vector λ in the one-dimensional null space of A^T.
3. Construct the polynomial $g(\alpha, \beta) = \lambda^T F(x_0 + \alpha q_1 + \beta q_2, \mu_0 + \alpha u_1 + \beta u_2)$.
4. Construct the Hessian matrix H of g and compute the two solutions (α_1, β_1) and (α_2, β_2) of the polynomial system

$$\begin{aligned} [\alpha, \beta] \cdot H(0,0) \cdot [\alpha, \beta]^T &= 0 \\ \alpha u_1 + \beta u_2 &= \Delta_\mu \end{aligned}$$

Return $\Delta x_1 := \alpha_1 q_1 + \beta_1 q_2$ and $\Delta x_2 := \alpha_2 q_1 + \beta_2 q_2$.

After computing the tangent direction for the nonradially symmetric solution branch, the last step is to track along that solution branch using the tangent direction as a first order description of the solution branch locally. After successfully moving off of the singularity and onto a smooth point on the solution branch, standard predictor-corrector methods were used to track along the solution branch. Figure 3.2 pictorially demonstrates the local behavior of the solution branches near the bifurcation at μ_2 for the running example. Figures 3.3 and 3.4 show the progression of the nonradial solution in each direction along the nonradially symmetric solution branches. Even though the figures indicate that the "upper" and "lower" solution branches appear to differ only by a rotation, numerical values suggest that this is not the case and the next section shows that they indeed behave very differently.

4. Linear stability study. An important question is to determine the stability of the solution branches that we have computed. To that end, define $U^n = (\sigma_1(n\tau), p_1(n\tau), R_1(n\tau)), \rho_1(n\tau))$ where τ is the time step size. We solved the lin-

FIG. 3.2. *Local behavior of the solution branches*

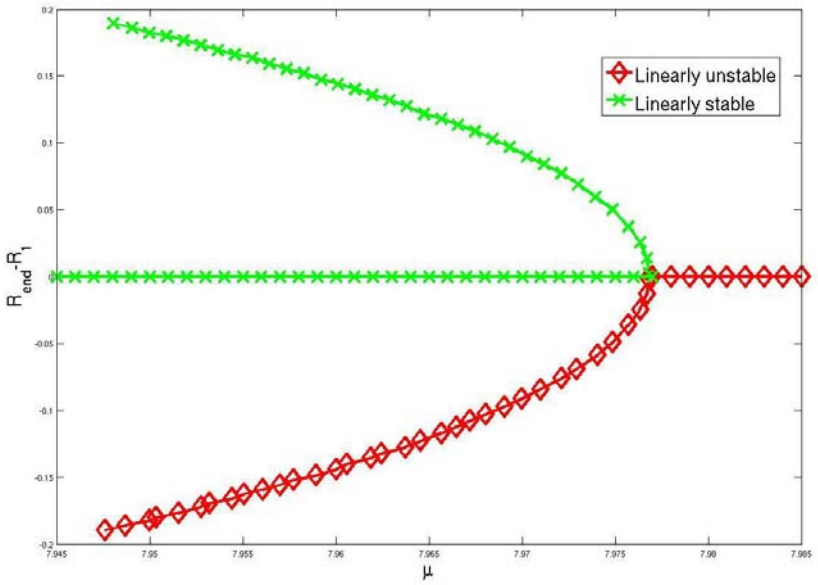

earized system described in [21] using a third order scheme in the spatial direction coupled with the backward Euler scheme in time direction. Such a scheme is unconditional stable. At each time step, this required the solving of the linear system $U^{n+1} = AU^n$, where the matrix A depends on the steady state solutions (σ_0, p_0, R_0, ρ_0, see [21] for the detail) and τ. In particular, this process transfers the linear stability of the solution to the spectrum of the matrix A which depends upon the solution.

Let $|\rho(A)|$ denote the maximum absolute value of the eigenvalues of A. If $|\rho(A)| < 1$, then $\|U^n\| \to 0$ yielding a stable system. Additionally, if $|\rho(A)| > 1$, then the system is unstable. Since the stability of the radially symmetric solutions has been determined [21], we are interested in the stability of the nonradially symmetric solution branches.

For the working example, namely $R = 2.5$ and $\underline{\sigma} = 0.5$, we computed the eigenvalues of A for different values of μ along the "upper" and "lower" nonradially symmetric solution branches to determine the stability. Tables 4.1 and 4.2 list $|\rho(A)|$ along the "upper" and "lower" branches, respectively. In particular, when $7.86654 < \mu < \mu_2 \approx 7.97689$, the "upper" branch is stable and, for μ near μ_2, the "lower" branch is unstable, as pictorially presented in Figure 3.2. This computation shows that the top two solutions in Figure 3.3 are stable while all the other solutions in Figures 3.3 and 3.4 are unstable.

Since $|\rho(A)|$ is close to 1 for some of these computations, we verified the accuracy computations by doubling the number of grid points three times. The results of this computation are presented in Table 4.3. In particular, the results described in this table together with Table 3.2 suggest that our numerical approximations have error on the order of 10^{-6} yielding that the linear stability is convincing and reasonable. Moreover, eigenvalue analysis is matched by time marching in our numerical simulation. FIG 4.1 shows the nonlinear stability for $\mu = 7.882432$ ($|\rho(A)| = 0.99998$) and

FIG. 3.3. *Nonradially symmetric "upper" branch*

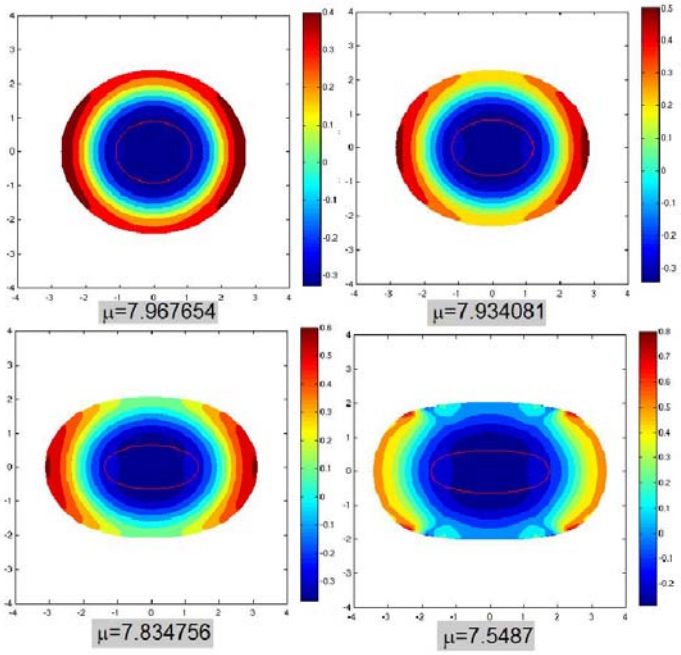

TABLE 4.1
Maximum eigenvalue for the "upper" branch

μ	$\lvert\rho(A)\rvert$	μ	$\lvert\rho(A)\rvert$	μ	$\lvert\rho(A)\rvert$
7.976889	1.00000	7.926135	0.99994	7.707620	1.00823
7.975754	0.99999	7.918189	0.99994	7.691728	1.03423
7.973053	0.99996	7.910243	0.99995	7.675836	1.06282
7.970353	0.99995	7.898324	0.99996	7.659944	1.09445
7.967654	0.99994	7.882432	0.99998	7.644052	1.12956
7.964954	0.99994	7.866540	1.00001	7.628160	1.16867
7.962254	0.99993	7.850648	1.00003	7.612268	1.21240
7.959554	0.99993	7.834756	1.00006	7.596376	1.26151
7.956854	0.99993	7.818864	1.00010	7.580484	1.31690
7.954154	0.99993	7.802972	1.00013	7.564592	1.37974
7.951454	0.99993	7.787080	1.00017	7.548700	1.45148
7.948754	0.99993	7.771188	1.00022	7.532808	1.53399
7.946054	0.99993	7.755296	1.00027	7.516916	1.62972
7.934081	0.99993	7.739404	1.00032	7.501024	1.74191

$\mu = 7.976203$ ($|\rho(A)| = 1.00002$).

5. Conclusion. In this paper, we have studied a model for the growth of a tumor with a necrotic core. The model has incorporated important physical quantities such as internal tumor pressure and cell-to-cell adhesion. We presented a numerical algebraic geometric approach based on homotopy continuation to solve the steady

FIG. 3.4. *Nonradially symmetric "lower" branch*

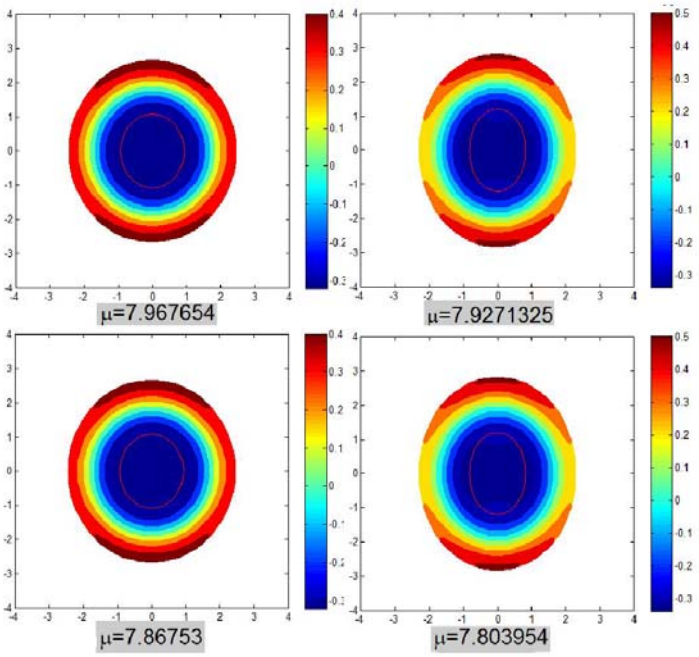

TABLE 4.2
Maximum eigenvalue for the "lower" branch

μ	$\lvert\rho(A)\rvert$	μ	$\lvert\rho(A)\rvert$	μ	$\lvert\rho(A)\rvert$
7.976889	1.00000	7.927133	1.00022	7.708590	1.08048
7.976203	1.00002	7.919186	1.00024	7.692696	1.10909
7.973553	1.00004	7.911239	1.00027	7.676802	1.14047
7.970903	1.00006	7.899318	1.00030	7.660908	1.17498
7.968253	1.00007	7.883424	1.00035	7.645014	1.21299
7.965603	1.00009	7.867530	1.00041	7.629120	1.25499
7.962953	1.00010	7.851636	1.00046	7.613226	1.30154
7.960303	1.00011	7.835742	1.00051	7.597332	1.35331
7.957653	1.00012	7.819848	1.00057	7.581438	1.41114
7.955003	1.00013	7.803954	1.00063	7.565544	1.47604
7.952353	1.00014	7.788060	1.00069	7.549650	1.54927
7.949703	1.00015	7.772166	1.00075	7.533756	1.63242
7.947053	1.00015	7.756272	1.00869	7.517862	1.72754
7.943027	1.00017	7.740378	1.03051	7.501968	1.83724

state system and numerical compute nonradially symmetric solution branches. The linear stability analysis reveals that the stability of steady state solution depends on the aggressiveness parameter μ of the model. In summary, this approach provides a general method to study tumor growth systems with free boundaries.

FIG. 4.1. *Nonlinear stability*

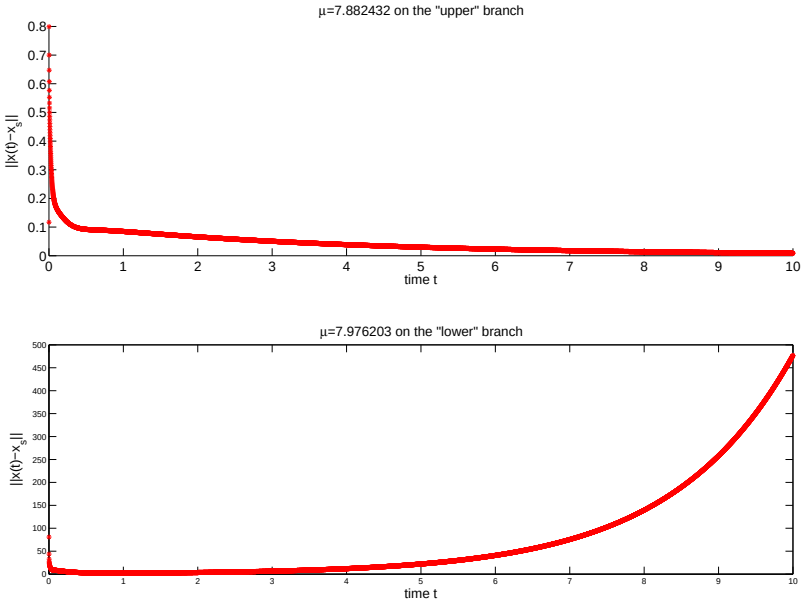

TABLE 4.3
Errors and orders

Formula	value
$\max \lvert x_{10} - x_{20} \rvert$	$7.9414e{-6}$
$\max \lvert x_{10} - x_{40} \rvert$	$7.4104e{-6}$
$\max \lvert x_{20} - x_{40} \rvert$	$6.0829e{-7}$
$\max \lvert x_{10} - x_{80} \rvert$	$7.3657e{-6}$
$\max \lvert x_{20} - x_{80} \rvert$	$6.5529e{-7}$
$\max \lvert x_{40} - x_{80} \rvert$	$4.4882e{-8}$
$\log_2 \left(\frac{\lVert x_{10} - x_{80} \rVert_2}{\lVert x_{20} - x_{80} \rVert_2} \right)$	2.6507
$\log_2 \left(\frac{\lVert x_{20} - x_{80} \rVert_2}{\lVert x_{40} - x_{80} \rVert_2} \right)$	2.7477

REFERENCES

[1] J.A. ADAM, General aspect of modeling tumor growth and immune response, A Survey of Models for Tumor-Immune System Dynamics (J.A.Adam and N. Bellomo, eds.) Birkhäuser, Boston, 14–87, (1996).

[2] J.A. ADAM AND S.A. MAGGELAKIS, Diffusion regulated growth characteristics of a spherical prevascular carcinoma, *Bull. Math. Biol.*, Vol 52, 549–582, (1990).

[3] D.J. BATES, J.D. HAUENSTEIN, A.J. SOMMESE, AND C.W. WAMPLER, Bertini: Software for numerical algebraic geometry. Available at www.nd.edu/∼sommese/bertini.

[4] D.J. BATES, J.D. HAUENSTEIN, A.J. SOMMESE, AND C.W. WAMPLER, Adaptive multiprecision path tracking, *SIAM Journal on Numerical Analysis* Vol. 46, 722–746, (2008).

[5] D.J. BATES, J.D. HAUENSTEIN, A.J. SOMMESE, AND C.W. WAMPLER, Stepsize control for path tracking, *Contemporary Mathematics* Vol. 496, 21–31, (2009).

[6] B. Bazally and A. Friedman, Global existence and asymptotic stability for an elliptic-parabolic free boundary problem: an application to a model of tumor growth, *Indiana Univ. Math. J*, Vol 52, 1265–1304, (2003).
[7] N. Britton and M.A.J. Chaplain, A qualitative analysis of some models of tissue growth, *Math. Biosci.*, Vol 113, 77–89, (1993).
[8] H.M. Byrne and M.A.J. Chaplain, Growth of nonnecrotic tumors in the presence and absence of inhibitors, *Math. Biosci.*, Vol 130, 151–181, (1995).
[9] H.M. Byrne and M.A.J. Chaplain, Modelling the role of cell-cell adhesion in the growth and development of carcinomas, *Mathl. Comput. Modelling*, Vol 12, 1–17, (1996).
[10] M.A.J. Chaplain, The development of a spatial pattern in a model for cancer growth, *Experimental and Theoretical Advances in Biological Pattern Formation* (H.G. Othmer, P.K. Maini, and J.D. Murray, eds), Plenum Press, 45–60, (1993).
[11] M. G. Crandall and P. H. Rabinowitz, Bifurcation from simple eigenvalues, *J. Funct. Anal.*, Vol 8, 321 C 340, (1971).
[12] S. Cui and A. Friedman, Analysis of a Mathematical Model of the Growth of Necrotic Tumors, *Journal of Mathematical Analysis and Applications* 255, 636–677, (2001).
[13] S. Cui and J. Escher ,Bifurcation Analysis of an Elliptic Free Boundary Problem Modelling the Growth of Avascular Tumors, *SIAM Journal on Mathematical Analysis* Vol 39, 210-235 (2007)
[14] S. Cui and J. Escher ,Asymptotic Behaviour of Solutions of a Multidimensional Moving Boundary Problem Modeling Tumor Growth, *Communications in Partial Differential Equations* Vol 32, 636 - 655 (2008)
[15] M. Fontelos and A. Friedman, Symmetry-breaking bifurcations of free boundary problems in three dimensions, *Asymptotic Analysis*, Vol 35, 187–206, (2003).
[16] A. Friedman and B. Hu, Bifurcation from stability to instability for a free boundary problem arising in a tumor model *Arch. Rat. Mech. Anal.*, Vol. 180, No. 2, (2006).
[17] A. Friedman and F. Reitich, Analysis of a mathematical model for growth of tumor, *J. Math. Biology*, Vol 38, 262–284, (1999).
[18] A. Friedman and F. Reitich, Nonlinear stability of a quasi-static Stefan problem with surface tension: A continuation approach, *Ann. Scoula Norm. Sup. Pisa Cl. Sci.,*, Vol. 30(4), pp. 341–403,(2001).
[19] H.P. Greenspan, Models for the growth of a solid tumor by diffusion, *Studies Appl. Math*, Vol 52, 317–340, (1972).
[20] H.P. Greenspan, On the growth of cell culture and solid tumors, *Theoretical Biology*, Vol 56, 229–242, (1976).
[21] W. Hao, J.D. Hauenstein, B. Hu, Y. Liu, A.J. Sommese, and Y.-T. Zhang Bifurcation of steady-state solutions for a tumor model with a necrotic core *submitted: available at www.nd.edu/∼sommese/preprints*
[22] S.A. Maggelakis and J.A. Adam, Mathematical model for prevasculat growth of a spherical carcinoma, *Math. Comp. Modeling*, Vol 13, 23–38, (1990).
[23] D.L.S. McEwain and L.E. Morris, Apoptosis as a volume loss mechanism in mathematical models of solid tumor growth, *Math. Biosci.*, Vol 39, 147–157, (1978).
[24] A.J. Sommese and C.W. Wampler, *Numerical solution of systems of polynomials arising in engineering and science*, (2005), World Scientific Press, Singapore.